ELECTRON TRAPPING IN EVOLVING CORONAL STRUCTURES DURING A LARGE GRADUAL HARD X-RAY/RADIO BURST

G. BRUGGMANN
Institute of Applied Physics, University of Bern, Switzerland

N. VILMER, K.-L. KLEIN
DASOP, Observatoire de Paris, Section d'Astrophysique de Meudon, France

and

S. R. KANE
Space Sciences Laboratory, University of California, Berkeley, CA, U.S.A.

(Received 2 March, 1993; in revised form 24 June, 1993)

Abstract. Gradual hard X-ray/radio bursts are characterized by their long duration, smooth time profile, time delays between peaks at different hard X-ray energies and microwaves, and radiation from extended sources in the low and middle corona. Their characteristic properties have been ascribed to the dynamic evolution of the accelerated electrons in coronal magnetic traps or to the separate acceleration of high-energy electrons in a 'second step' process. The information available so far was drawn from qualitative considerations of time profiles or even only from the common occurrence of emissions in different spectral ranges. This paper presents model computations of the temporal evolution of hard X-ray and microwave spectra, together with a qualitative discussion of radio lightcurves over a wide spectral range, and metric imaging observations. The basic hypothesis investigated is that the peculiar 'gradual' features can be related to the dynamical evolution of electrons injected over an extended time interval in a coronal trap, with electrons up to relativistic energies being injected simultaneously. The analyzed event (26 April, 1981) is particularly challenging to this hypothesis because of the long time delays between peaks at different X-ray energies and microwave frequencies. The observations are shown to be consistent with the hypothesis, provided that the electrons lose their energy by Coulomb collisions and possibly betatron deceleration. The access of the electrons to different coronal structures varies in the course of the event. The evolution and likely destabilisation of part of the coronal plasma-magnetic field configuration is of crucial influence in determining the access to these structures and possibly the dynamical evolution of the trapped electrons through betatron deceleration in the late phase of the event.

1. Introduction

Accelerated particles in the solar corona are revealed by their radiative signatures, especially γ-ray, hard X-ray, and radio waves. Flare-associated hard X-ray and radio emissions typically last between tens of seconds and several tens of minutes. Based on the different durations, two extreme cases of flares have been distinguished: 'impulsive' and 'gradual' (or 'extended') hard X-ray/radio bursts. Gradual events share a number of common properties which allow one to distinguish them from the more frequent impulsive flares (cf. reviews by Dennis, 1985; Tanaka, 1987; Dennis, 1988):

– smooth time profiles;

– delays of the high-energy X-ray peaks with respect to low energies and of microwaves with respect to X-rays, or hardening of the hard X-ray spectrum (e.g.,

Solar Physics **149:** 171–193, 1994.

Bai and Dennis, 1985; Cliver *et al.*, 1986);

– association with Hα flares of large area and emission from extended magnetic structures in the corona as evidenced by X-ray and microwave images (Ohki *et al.*, 1983; Takakura *et al.*, 1983; Tsuneta *et al.*, 1984; Bai and Dennis, 1985; Kawabata *et al.*, 1982; Kosugi, Kai, and Suzuki, 1983), by the low-frequency turnover of the microwave spectrum (Cliver *et al.*, 1986; Kai *et al.*, 1986), and by the association with decimetric to decametric radio continua (Kai *et al.*, 1983; Klein *et al.*, 1983; Cliver, Kahler, and McIntosh, 1983; Pick, 1986; Trottet, 1986);

– association with large-scale perturbations of the coronal magnetic field and plasma configuration, as revealed by, e.g., erupting filaments, coronal mass ejections (Cliver *et al.*, 1986) or moving type IV bursts (Klein *et al.*, 1983);

– a high ratio of microwave-to-hard X-ray peak emission ('microwave richness'; Kai, Kosugi, and Nitta, 1985; Cliver *et al.*, 1986).

The distinction between impulsive and gradual hard X-ray/radio bursts is not always evident; Nakajima (1983), using microwave imaging and hard X-ray spectral observations, showed that gradual and impulsive signatures may occur *simultaneously*, but at different locations. This underlines the influence of the environment where the emission is produced on the temporal and spectral evolutions of the radiation.

The above associations between different radiative signatures have been derived from qualitative studies that compared time profiles in different spectral ranges, or have been deduced from global information such as the mere occurrence of different types of metric emissions. Based on such studies the idea arose that a different acceleration mechanism accounts for this type of flare as compared with impulsive events (e.g., Bai, 1982; Bai *et al.*, 1983; Cliver *et al.*, 1986; Bai and Sturrock, 1989). The suggestion that the extended coronal shock wave revealed by metric type II bursts might be the accelerator was later refuted by X-ray imaging (Kahler, 1984; Ohki *et al.*, 1983; Cliver *et al.*, 1986) and by a more thorough consideration of the radio emissions (Klein *et al.*, 1983, 1988; Trottet, 1986). The hypothesis of different acceleration processes competes with the suggestion that because of the different environment in which the gradual hard X-ray/radio emissions occur, the accelerated particle distributions evolve in a different way than during impulsive events. One difference between the impulsive and gradual events could be that electrons are more efficiently trapped in coronal structures during gradual hard X-ray/radio bursts (Bai and Ramaty, 1979; Vilmer, Kane, and Trottet, 1985; Vilmer, 1987; Kosugi, Dennis, and Kai, 1988; Dennis, 1988).

In the present paper we investigate the hypothesis that, irrespective of the acceleration process, the interactions of the nonthermal electrons with the ambient plasma are responsible for the characteristic features of gradual events. The aim of the study is threefold:

(1) to deduce through a detailed analysis of the spectral evolution in the hard X-ray and microwave range properties of the energetic electrons and the parameters at the site of emission;

(2) to specify the link between gradual signatures at different wavelengths and the different electron populations involved as well as the role of the magnetic structure and its evolution in the course of the flare development;

(3) to compare the energy budgets of the suprathermal electrons during gradual and impulsive hard X-ray/radio events.

The gradual event of 26 April, 1981 at ~11:40 UT is particularly challenging because of the pronounced time delays of tens of seconds up to several minutes detected between the peak times at different photon energies and microwave frequencies. The study relies on spectrographic observations in the hard X-ray and radio range (centimetric to metric), numerical models of hard X-ray and microwave emission, and imaging at metric wavelengths. Section 2 presents the observations and the quantitative analysis of the hard X-ray and microwave emissions in terms of electrons trapped in coronal magnetic structures. Peak time delays between different hard X-ray channels are established by a statistical analysis in Section 2.2.1, and parameters of the coronal trap are inferred. The parameters describing the energetic electron population are then derived through the modelling of the hard X-ray emission, assuming bremsstrahlung (Section 2.3). In Section 2.4 we discuss metre wave images of the corona above the flare site. They demonstrate that electrons are injected into evolving large-scale magnetic field structures. This information is used in Section 2.5 to compute the microwave emission of the electron population that radiates the hard X-rays. The results are compared with the information inferred by similar model computations for other flares, both impulsive and gradual, in Section 3, and confronted with proposed scenarios of gradual hard X-ray/radio bursts.

2. Observations

2.1. Overview

The event of 26 April, 1981, starting at 11:40 UT, was a large gradual hard X-ray/microwave burst (Dennis, 1985; Cliver *et al.*, 1986) and was also reported as a gamma-ray line flare (Bai and Dennis, 1985). Large microwave fluxes were observed up to 35 GHz. Hα observatories report a limb flare of importance 2, with a large dispersion of onset times between 10:57 and 11:39 UT. The flare occurs around N16 W75, in a very extended active region. Two eruptive prominences off the west limb were observed in Hα from 11:12 to 11:54 UT and from 12:25 to 12:46 UT. The flare was also associated with a coronal mass ejection (Cliver *et al.*, 1986). GOES reported an X1.2 soft X-ray event lasting from 10:57 to 14:16 UT and peaking at 12:25 UT. In the radio range groups of type III bursts occurred between 30 and 130 MHz prior to the gradual event under discussion (from 11:33 to 11:44 UT; Weissenau). At metric and decimetric wavelengths the counterpart of the gradual hard X-ray/microwave burst was observed as an intense type IV burst (Weissenau, Dwingeloo – *Solar Geophysical Data*; Nançay).

Cliver *et al.* (1986) suggested that the burst under study is the gradual phase

of the impulsive hard X-ray event at 11:16 UT. While the fact that the prominence eruption starting at 11:12 UT continues late into the second flare might argue in favour of this hypothesis, the observation of type III burst groups from 11:33 to 11:44 UT shows that impulsive electron acceleration occurs much closer to the onset of the gradual burst. The low-frequency range of the type III bursts might suggest that the impulsive acceleration takes place higher in the corona than commonly observed. In the following we consider only the gradual burst. Whether it is preceded by an impulsive phase starting 30 or 10 min before is not essential in this discussion. However, the presence of evolving coronal structures revealed, e.g., by the prominence eruption will turn out as an important feature. The analysis will use microwave observations between 3.2 and 35 GHz from Bern and ISEE-3 hard X-ray data between 20 and about 200 keV as shown in Figure 1, as well as decimetric/metric data from Bordeaux (courtesy J. M. Robillot) and Nançay, including imaging observations of the Nançay radioheliograph.

The microwave event is extraordinarily intense (Figure 1). The peak flux density is $\simeq$2800 s.f.u. at 35 GHz. The microwave richness index of 12.8, as defined in Bai and Dennis (1985), is very high. The spectral maximum is situated around 5.2 GHz. The circular polarization is between 0 and 15% for all the frequencies. A remarkable feature of the hard X-ray emission is the peak time delay of the order of 100 s seen between the 20–38 and 105–142 keV channels (Figure 1). Delays between the lowest energy hard X-ray peaks and the microwave peaks are even larger: 330 s for 3.2 GHz and 480 s for 35 GHz (cf. Figure 1).

2.2. Peak delays between lightcurves at different photon energies

2.2.1. Correlation Study of Hard X-Ray Lightcurves

The present analysis of the hard X-ray event addresses photon energies greater than 20 keV, for which the thermal bremsstrahlung contribution is not the dominant component. As shown in Figure 1, the hard X-ray emission above 20 keV has essentially a smoothly varying time profile. Nevertheless, different subpeaks can be distinguished in the lightcurves. In order to quantitatively estimate the energy dependence of the delays between hard X-ray peaks at high and low energies, cross-correlation coefficients between the X-ray counting rates have been computed (Vilmer *et al.*, 1987). The resulting delays with the uncertainties on their values obtained through this method are shown in Figure 2.

The correlation study confirms the delays of the order of several tens to 100 s suggested by the lightcurves. In order to investigate to which extent the interaction of the energetic electrons with the ambient plasma can account for the delays, we model the hard X-ray emission from a population of electrons which is injected simultaneously at all energies over a finite duration and perfectly trapped in a coronal magnetic structure.

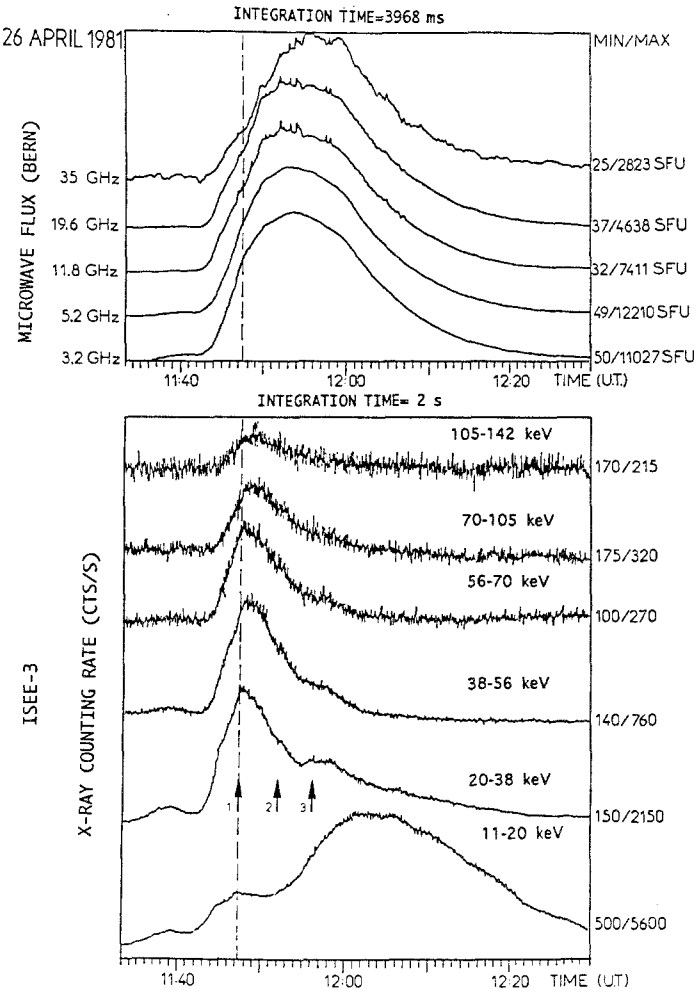

Fig. 1. ISEE-3 X-ray and microwave (Bern) time profiles for the 26 April, 1981 event. High-energy X-ray peak times are delayed by up to 100 s, microwave peaks by up to 8 min with respect to the 20–38 keV X-ray channel (see the dashed line indicating the peak time at 20–38 keV). The peak times of the different injections of Table I are indicated by arrows.

2.2.2. Parameters of the Coronal Trap Derived from the Hard X-Ray Emission

Based on the models described in Vilmer, Kane, and Trottet (1982), MacKinnon *et al.* (1983), and Trottet and Vilmer (1983, 1984) we consider the time-extended injection of nonthermal electrons into a region of uniform density (n_0) of cold electrons and protons. The injection function is described by a power-law in energy, with constant index δ and varying amplitude $q_0 f(t)$:

$$q(E, t) = q_0 f(t) E^{-\delta} , \tag{1}$$

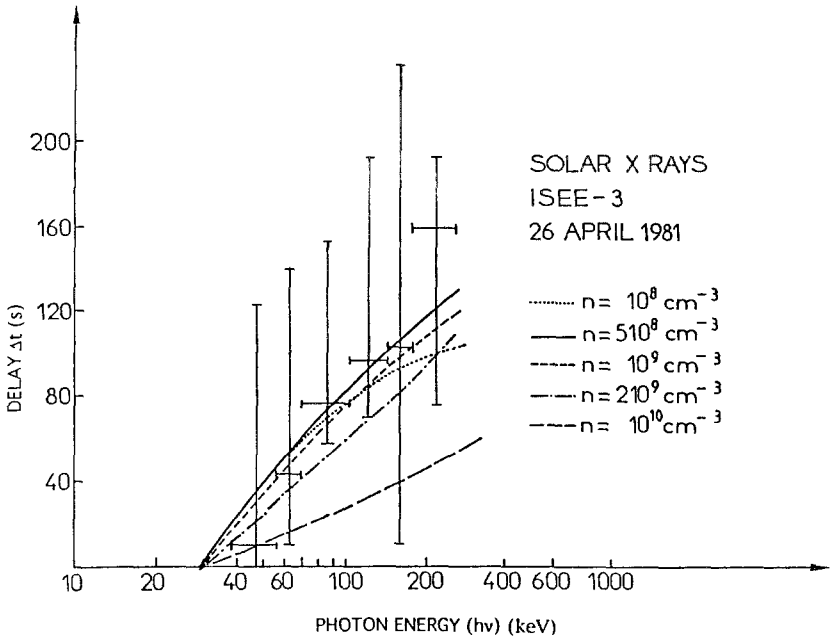

Fig. 2. Comparison of observed (error bars) and computed delays $\Delta t(h\nu)$ as a function of the photon energy $h\nu$.

where $f(t)$ is assumed to be a parabola for $t_s < t < t_0 + t_s$ and 0 elsewhere. At all energies the injection function has a maximum at $t_{\max} = t_s + t_0/2$. The evolution of the electrons in the source is supposed to be governed by collisions with the ambient electrons. Under the assumption of perfect trapping the total hard X-ray flux depends on the parameters n_0, δ, q_0, and t_0.

Assuming first a single parabolic injection the density n_0 accounting for the observed peak delays was estimated. These delays are weakly dependent on the electron injection spectrum (Vilmer, 1985), and the index δ is chosen in a first step as in a thick target model ($\delta = 3.5$). Furthermore, $t_{\max}$ is determined in a first trial by the duration at half the peak value of the lowest energy X-ray band for which the thermal contribution is not dominant, leading to $t_{\max} = 260$ s. The computed delays for a set of ambient densities are then plotted in Figure 2. It appears that a low value of the density $n_0 \leq 10^{10}$ cm^{-3}) is necessary to reproduce the observed energy dependence of the delay. This implies X-ray emission from the corona, which is consistent with imaging of other gradual hard X-ray bursts (Takakura *et al.*, 1983; Tsuneta *et al.*, 1984).

2.3. Quantitative analysis of the hard X-ray emission: parameters of the electron injections

Due to the relative complexity of the temporal evolution of the emission, a single parabolic injection cannot reproduce the whole event. Following the idea of

TABLE I
Parameters of the electron injections: 26 April, 1981, 11:40–12:00 UT

Injection	1	2	3
Spectral index	3.6	4.3	4.5
Duration (s), $t_0 = 2t_{max}$	520	120	360
Starting time, t_s (UT)	11:42:40	11:50:40	11:53:00
Maximum time, t_m (UT)	11:47:00	11:51:40	11:56:00
n_0 (cm^{-3})	10^9	10^9	10^9
Total number of injected electrons ($E > 20$ keV)	14.4×10^{37}	3×10^{37}	5×10^{37}
Mean total electron flux ($E > 20$ keV) (s^{-1})	2×10^{35}	2.5×10^{35}	1×10^{35}

'elementary flare bursts' (de Jager and de Jonge, 1978) we decomposed the event from 11:43 to 12:00 UT into a series of successive continuous parabolic injections, each of them having a constant spectral index, δ_i, during the whole injection. Figures 3(a–c) compare the observed and computed time profiles at selected photon energies, showing that the three injections allow us to reproduce the essential features of the hard X-ray lightcurves. The peak times of these injections are indicated by the arrows in Figures 1 and 3(a–c). The best parameters of each injection are determined by computing the X-ray flux produced by all the electrons already injected and comparing it with the X-ray observations. It is assumed furthermore that the mean density of ambient electrons in the X-ray source is the same for the three injections and does not vary with time during each injection. This assumption will be discussed in Section 3.1. The resulting parameters, as well as the total number of energetic electrons with energies greater than 20 keV provided during each injection are shown in Table I. Observed and calculated photon spectra shortly after the maximum of the first injection and well in the declining phase of the third injection are plotted in Figures 3(d) and 3(e). Given the rather low number of free parameters (1 parameter to describe the medium and 12 to describe the three injections) compared with the number of fitted data points ($\simeq$200) we consider that the computed X-ray fluxes at different energies are in satisfactory agreement with the observations. We conclude that the hard X-ray emission is consistently explained by a time-extended injection of a population of nonthermal electrons into a low-density trap. It is to be noted that a combination of time-extended injection and trapping is required to explain the observed delays.

2.4. THE CORONA ABOVE THE FLARING ACTIVE REGION: EVIDENCE FOR ELECTRON INJECTION INTO LARGE-SCALE STRUCTURES

In this section we discuss the imaging observations at 169 MHz, together with radio and hard X-ray lightcurves over a large bandwidth, in a quest for information on the spatial structure of the emitting sources.

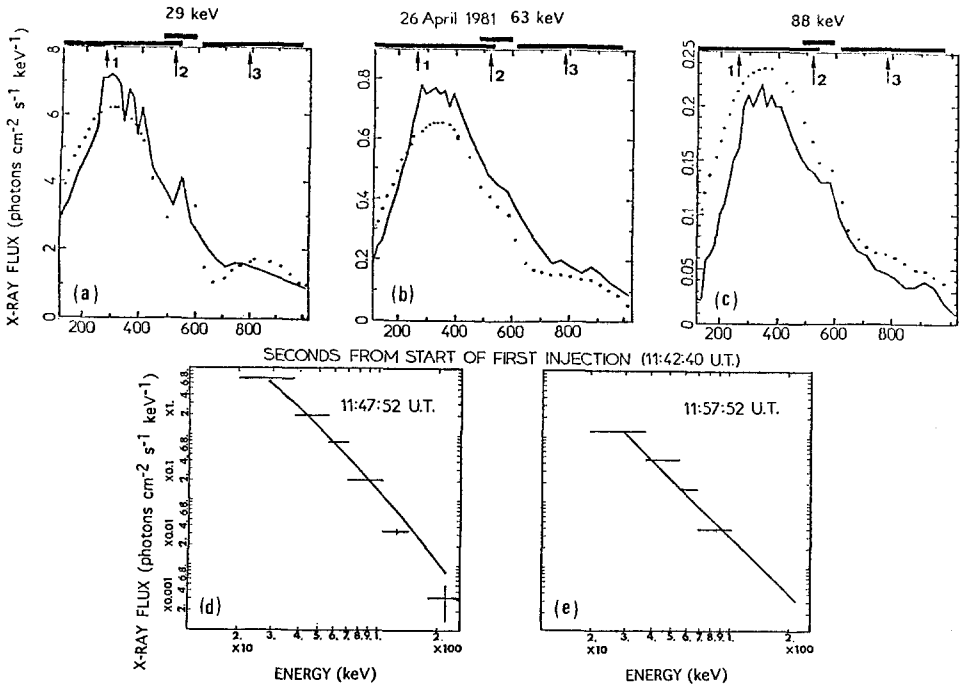

Fig. 3. (a–c) Comparison of observed (solid line) and computed (dotted line) time profiles for the 29, 63, and 88 keV X-ray fluxes. The peak times of the different injections of Table I are indicated by arrows. Durations of each injection are also indicated by thick bars on top of the frames. (d, e) Observed X-ray spectra for two different instants during the 26 April, 1981 event. Also shown for comparison are the computed spectra for the parameters given in Table I (solid line).

Inspection of the lightcurves (Figures 1 and 4(b)) shows that the emission from hard X-rays to metric wavelengths rises around 11:43 UT. At frequencies below about 300 MHz intense emission from a preceding flare masks the onset. The radioheliographic observations at 169 MHz show that emission rises simultaneously in two different regions at 11:43 UT. The emitting sources are close to those of the remnant of the preceding flare. They are stable until 11:48 UT. The positions and diameters (FWHM) of the sources as observed with the east–west and the north–south branches of the Nançay radioheliograph (NRH) are plotted in Figure 4(a). The lightcurves of the two sources are given in the top panel of Figure 4(b). The north-eastern (NE in Figure 4) source overlies the region where active region prominences are reported to erupt between 11:12 and 11:54 UT and 12:25 and 12:46 UT, respectively. While both 169 MHz sources are seen to brighten simultaneously at 11:43 UT, their subsequent evolution is different: the south-western source declines before the maximum of the first electron injection identified in hard X-rays, while the north-eastern source stays bright throughout the first injection and fades soon after the start of the second injection. It therefore appears that the different injections of electrons identified in the hard X-ray analysis have different

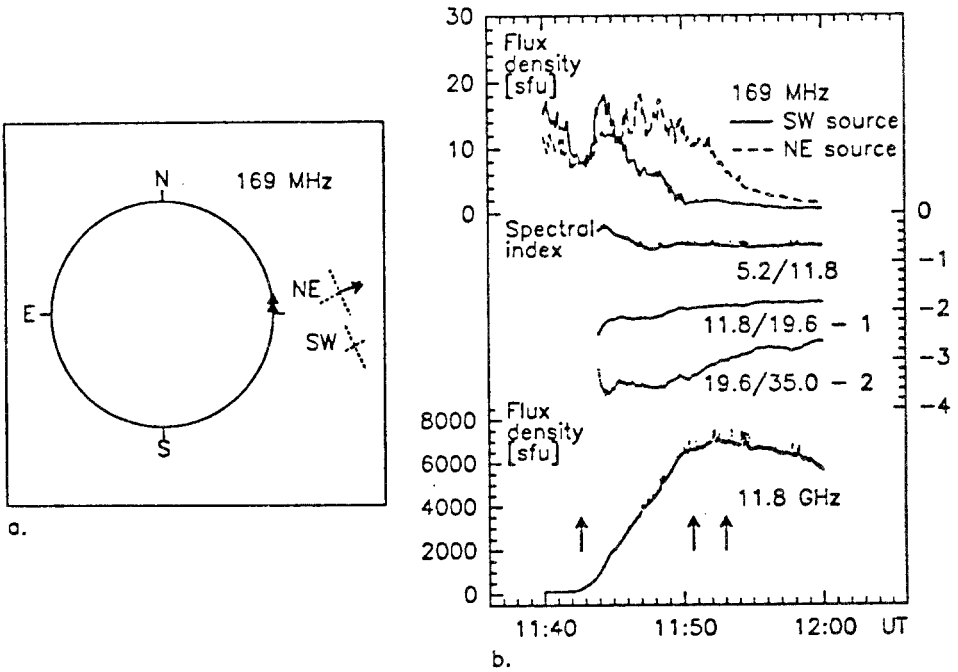

Fig. 4. (a) Map of the meter-wave sources in the 26 April, 1981 event after 11:43 UT observed with the Nançay radioheliograph (NRH) at 169 MHz. The diameters measured separately with the east-west and north-south branches of the Nançay radioheliograph are plotted as dashed line segments (full width at half maximum). The arrow indicates the direction and range of the motion of the north-eastern source in the late phase of the event (cf. Section 2.4). The circle outlines the optical disk of the Sun, the two black triangles give the positions of erupting prominences reported from 11:12 to 11:54 (southern triangle) and 12:25 to 12:46 UT (northern t.) in *Solar Geophysical Data*. (b) Time histories of the radio flux densities (*top*: two sources resolved by the NRH at 169 MHz, *bottom*: whole-Sun flux, Bern University polarimeter at 11.8 GHz) and the microwave spectral indices (Bern single-frequency polarimeters) between 5.2, 11.8, 19.6, and 35 GHz, respectively. The spectral indices at high frequencies have been reduced as indicated on the figure for the convenience of easy graphic representation. The arrows at the bottom of the figure mark the start of the three electron injections identified in hard X-rays.

responses in the radio emission produced in the middle corona. While on the one hand the NRH observations confirm the existence of different episodes of particle injection, they suggest on the other hand that the electrons provided during the three injections do not have access to the same structures in the middle corona. This could be linked with the destabilisation of the large-scale coronal structure involved in the metre-wave emission. Indeed the north-eastern source suddenly starts moving outward at 11:48 UT, and this movement can be tracked until 11:53 UT. The speed projected onto the plane of the sky is 500 km s^{-1}. The direction and range of this motion are given by the arrow in Figure 4(a). The 169 MHz emission fades during this moving phase and does not rise afterwards, contrary to the radio emission at decimetric wavelengths. At 408 MHz (Nançay: spectrograph of the Space Research Department of Meudon Observatory) and 930 MHz (Bordeaux)

the second and third injection identified in hard X-rays lead to a new rise, which starts at 11:57 UT and is more pronounced at the higher frequency. This shows that electrons continue to be injected in a wide, but more restricted range of altitudes than before.

Differences between the three electron injections are also identified in the microwave data: inspection of the spectral index α (flux density $\sim\nu^{\alpha}$; middle panel of Figure 4(b)) shows that the spectral index above 11 GHz is essentially constant during most of the first injection, but that relatively more microwave emission comes from the high frequencies during the second and third injection than during the first one. This effect does not appear in the same manner between 5.2 and 11.8 GHz, presumably because 5.2 GHz is not optically thin. The evolution of the microwave spectral index can be explained either by a hardening of the electron spectrum during the second and third injection, which is contradicted by the hard X-ray analysis (Table I), or by injection into regions of stronger magnetic field after 11:50 UT. The latter interpretation fits well within the picture of different coronal structures being accessible during different phases of the event under discussion.

2.5. Microwave emission from the nonthermal electrons in the hard X-ray source

In the light of the foregoing discussion we suppose that the microwaves are emitted by the electrons that also generate the hard X-ray emission, and in the same coronal structures. In order to check the quantitative consistency with the observations, we compute the gyrosynchrotron emission from these electrons, using the numerical model described by Klein (1987), which is based on the formalism developed by Ramaty (1969). For simplicity we continue to assume a uniform source (especially a uniform magnetic field). As shown in Klein, Trottet, and Magun (1986, Figure 2) this approach is expected to be acceptable for the description of the microwave spectrum at high frequencies, where self-absorption is negligible. In the case of the 26 April, 1981 event the frequencies 11.8, 19.6, and 35 GHz are in this range, while 5.2 GHz is close to the spectral maximum and 3.2 GHz in the optically thick range. At these low frequencies emission is expected to come from an extended source over which the magnetic field varies appreciably.

As the ambient density and the injection spectrum of the energetic electrons are given by the hard X-ray model, the free parameters determining the microwave spectrum above the turnover frequency are the magnetic field(s) (intensity and viewing angle) in the emitting source(s) and the high-energy cutoff of the emitting electrons, while the surface and the column density of the nonthermal electrons determine the frequency above which self-absorption becomes insignificant. The product of surface and column density is the total number of energetic electrons, which is determined by the hard X-rays. Only this product is relevant to the optically thin flux density spectrum.

We proceeded by deriving the free parameters of the microwave source(s) through the computation of gyrosynchrotron spectra at different instants and their

TABLE II
Model parameters of the microwave sources

	Source 1	Source 2
Field strength (gauss)	50	240
Viewing angle (deg)	45	45
Surface (cm^2)	7.0×10^{18}	4.0×10^{16}

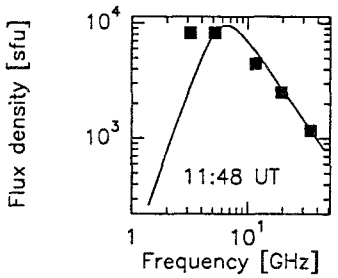

Fig. 5. Comparison of the computed (solid line) and the observed (full squares) microwave spectrum of the 26 April, 1981 event at 11:48:00 UT. The microwave source parameters were adjusted so as to represent the observed flux densities at frequencies at and above 5.2 GHz (in the least-squares sense).

comparison with the observations.

2.5.1. The First Electron Injection

Following the results of Section 2.4 we start with the microwave emission from the first injection of electrons. The instant at which the free parameters of the microwave source are determined was taken in the rising phase of the microwave emission such that the observed flux density be significant at all frequencies and that only the first of the three injections identified in the hard X-ray analysis contribute. The chosen instant was 11:48:00 UT (320 s after the start of the first injection). The observations of a spectral maximum at low frequencies together with a high flux density require an extended source region with a weak magnetic field. Field strengths ranging from 40 to 80 G yield an acceptable representation of the high-frequency spectrum, while higher field strengths imply a spectral turnover far above 5.2 GHz, in conflict with the observations. The values of field strength, viewing angle and source surface giving the best representation in the frequency range 5.2 to 35 GHz (in the least-squares sense, at 11:48 UT) are listed in column 2 ('source 1') of Table II. The computed flux density spectrum is plotted together with the observed one in Figure 5.

The electron injection spectrum was assumed to continue without break nor change of slope up to $E = 20$ MeV, above which value the gyrosynchrotron emission was found insensitive to a possible cutoff of the spectrum. In some

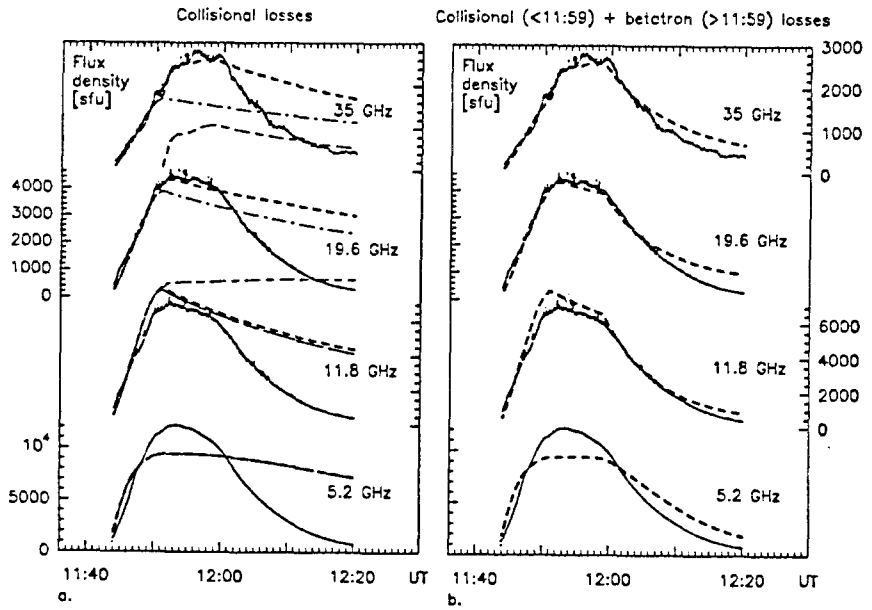

Fig. 6. Comparison of the computed (dashed lines) and observed time histories of the microwave fluxes in the case of pure collisional losses (a) and including betatron losses in the late phase of the event (b). The observed flux densities are represented by points that, because of the 1 s integration time, are mostly confounded into an apparently continuous line. In (a) the dashed-dotted lines represent the contribution of 'source 1', the long/short dashes that of 'source 2' of Table II. The emission from source 2 is not significant at 5.2 and 11.8 GHz. The fat dashes give the sum of the two sources. Only the sum of the two model sources is shown in (b).

comparable cases photon spectra have been reported to harden at about 400 keV (Yoshimori, Watanabe, and Nitta, 1985; Dennis, 1988). If in the considered case the electron spectra were harder than the spectrum derived from the hard X-ray analysis above, e.g., 400 keV, a weaker magnetic field would be required in the microwave source. This case is not examined here since there are no constraints from the X-ray data to argue in favour of or against a change of spectral slope at high electron energies.

The time evolution of the gyrosynchrotron radiation of the perfectly trapped electrons from injection 1 with the parameters of the microwave-'source 1' is plotted by dashed-dotted lines in Figure 6(a), together with the Bern observations, at four frequencies (solid line). A reasonable agreement between computations and observation is found in the rising phase of the emission at and above 11.8 GHz, until about 11:50 UT, and during the first half of the rising phase at 5.2 GHz. At 11:50 UT the computed gyrosynchrotron flux densities attain a maximum and then slowly decrease. The computed flux density spectrum is steeper than the observed one, which is seen as an increasing deficit of gyrosynchrotron emission towards higher frequencies above 11.8 GHz. After ~12:00 UT, however, in the declining phase of the observed emission, the computed flux density from the first

electron injection into 'source 1' exceeds the observed level. The difference increases throughout the declining phase, because Coulomb collisions in the constant low-density environment considered here are not an efficient loss mechanism for electrons of some hundreds to thousands of keV which radiate the microwaves. There must therefore be another mechanism of energy loss or particle precipitation in this late phase of the event or the density in the emitting region must increase, e.g., due to chromospheric evaporation. We conclude that:

(1) the rising phase of the microwave emission during injection 1 is satisfactorily described by the radiation of a trapped electron population in a spatially-extended coronal source which is also the seat of the hard X-ray emission;

(2) during the long-lasting phase of high flux density (until 12:00 UT) the observed high-frequency emission is more intense than the computed emission from the first electron injection, whereas the computed and observed emission at 11.8 GHz are in reasonable agreement;

(3) the microwave spectrum at and below 5.2 GHz is poorly represented by the model (with the exception of the early rising phase) because the observed flux density spectrum is not optically thin in that range and the source region was assumed homogeneous;

(4) an increasing excess of the computed (injection 1) with respect to the observed flux density occurs soon after the event starts to decline around 12:00 UT.

While there is no remedy to the unsatisfactory description of the low-frequency spectrum within a homogeneous gyrosynchrotron model, possible solutions to the deficiency at high frequencies (Section 2.5.2) and to the excess in the declining phase of the event (Section 2.5.3) are outlined in the following paragraphs.

2.5.2. The Second and Third Electron Injections

Following the qualitative analysis of the wide-band radio observations in Section 2.4, we consider that injections 2 and 3 provide electrons to low-lying coronal structures with stronger magnetic field than the model-source 1. For simplicity, we suppose in the following computations that no electrons are injected into source 1 during this phase. We further assume that the density of the ambient electrons is again 10^9 cm^{-3}. This assumption will be discussed in Section 3.1. The parameters of this new microwave source are determined through the requirement that the computed flux densities at 11.8, 19.6, and 35 GHz account for the observed excess at these frequencies above the contribution of 'source 1' at 11:52 UT. These parameters are given in the third column ('source 2') of Table II. As expected by the requirement that the new source contributes to the high-frequency emission only, hence that it is self-absorbed at frequencies below at least 11 GHz, the magnetic field is much higher than that of 'source 1'. As at the same time the flux density is moderate, the source must be more compact than 'source 1'. The time history of the computed gyrosynchrotron emission is plotted by the lines of long and short dashes (19.6 and 35 GHz) in Figure 6(a). The sum of the contributions from sources 1 and 2 is plotted as a fat dashed line. It is noted that the gyrosynchrotron spectrum

of 'source 2' is optically thick and that a uniform source model is not an adequate description of this situation. This restriction does not alter the requirement for a significant contribution of a source with stronger magnetic field than 'source 1'. It is plausible that the parameters of 'source 1' and 'source 2' describe a range of typical values rather than two separate structures.

2.5.3. *Temporal Evolution of the Microwave Emission after the End of the Particle Injections: Coulomb Collisions versus Betatron Deceleration*

The observed microwave emission continues for at least 20 min after the end of injection 3 identified in the hard X-rays. The rapidly varying components of the time profile at high frequencies during the declining phase may suggest a weak level of ongoing particle injections which are not efficient enough to be detectable in hard X-rays (note, however, that some of them show up in the X-ray data between 11 and 20 keV (Figure 1, e.g., 12:01 UT). On the other hand, Figure 6(a) shows that even if only the first electron injection is considered, the microwave emission from the region with $n_0 = 10^9$ cm^{-3} decreases much more slowly than the observations require. Coulomb collisions in this low density region are clearly not efficient enough to relax the population of high-energy electrons if it is perfectly trapped in a *static* magnetic structure. If significant quantities of electrons precipitated into the lower atmosphere, they should show up as short-lasting bursts in hard X-rays or microwaves. No such signature is seen in the hard X-ray observations. Rapid fluctuations exist at high microwave frequencies, but their flux density is far below that of the underlying slowly varying emission, and it is doubtful whether they are of solar origin (A. Magun, private communication). The smooth evolution at 0.93, 3.2, and 5.2 GHz also argues in favour of a slow energy loss rather than a sudden onset of particle precipitation.

Two alternative interpretations may be advocated: Coulomb collisions in a trap with increasing ambient density or losses due to the interaction of the fast particles with the magnetic field.

2.5.3.1. Coulomb Collisions in a Trap with Increasing Density. The decrease of the microwave emission is significantly more rapid when the density is enhanced. However, as long as $n_0 < 5 \times 10^9$ cm^{-3}, an excess above the observed flux density persists in the declining phase whilst a significant deficit occurs in the rising phase of the emission when $n_0 > 2 \times 10^9$ cm^{-3}. A variable ambient density, rising from an initial value of 10^9 cm^{-3} to more than five times that value in the decay phase might hence resolve the discrepancy between the observations and the static model computations. The density could be increased by chromospheric evaporation or due to the thermalization of the energetic electrons. These processes will be discussed in Section 3.1.

2.5.3.2. Betatron Deceleration. Electrons of high energies can lose energy through the emission of gyrosynchrotron radiation or through betatron decelera-

tion. Numerical tests show that gyrosynchrotron losses are insignificant on the time scales and in the weak magnetic fields under discussion. Betatron deceleration in a slowly expanding source volume does, however, provide an efficient loss mechanism which competes with collisional losses in that the expansion will tend to keep the ambient density on a low level. In the following, the effect of betatron deceleration is demonstrated with the formalism of Dulk (1973), assuming that the microwave source undergoes a self-similar expansion in all three directions during which the first and second adiabatic invariants are conserved. As shown by Dulk (1973, Figure 3), the increase of the source volume by a factor 8 will decrease the optically thin flux density by three to four orders of magnitude.

In order to evaluate the effect of betatron deceleration in the big microwave source, we consider the evolution of the electrons surviving from the first injection once the injection has ceased. To simplify the calculations we assume collisional losses in a static source until a time t_{exp} and subsequent expansion (without collisional deceleration) in each spatial direction. The linear expansion in each direction is described by the scale factor

$$\sigma(t) = 1 + a(t - t_{\mathrm{exp}}) \quad (t \geq t_{\mathrm{exp}}) \,, \tag{2}$$

where a is kept constant throughout the expansion. The magnetic field strength, the surface and the column density vary, respectively, as σ^{-2}, σ^{2}, σ^{-2}. a and t_{exp} are considered as free parameters determined through the comparison between computed and observed flux densities in the decay phase of the event, after 12:00 UT. The resulting flux density curves (sum of the contributions from the large expanding source 1 and the small static source 2) are plotted in Figure 6(b) for $a = 2 \times 10^{-4}$ s^{-1} and $t_{\mathrm{exp}} = 11:59$ UT. These values signify that the volume of the large microwave source increases by a factor 2.6 between the onset of the expansion and 12:20 UT. The abrupt decrease of the computed flux densities at t_{exp} seen in Figure 6(b) is an artifact due to the assumption of a sudden onset of the expansion at constant rate. An earlier onset with slowly increasing a would yield a smoother aspect of the computed flux density curves, and would allow for a better representation of the observations after 12:10 UT, too. Comparison of Figures 6(a) and 6(b) shows that the betatron deceleration is efficient enough to explain the observed decrease of the microwave emission. This does not exclude that small amounts of energy continue to be injected into the corona. The perturbation of the extended coronal structures, that presumably overlie the sites of hard X-ray and microwave emission, is witnessed by the moving type IV burst observed at 169 MHz. The occurrence of source motions during gradual hard X-ray/microwave bursts has also been reported from imaging observations (Kosugi, Kai, and Suzuki, 1983; Tanaka, 1987).

3. Discussion and Conclusions

A large gradual hard X-ray/radio burst has been analyzed by means of radiative diagnostics of the energetic electrons and of the structures in the middle corona that presumably overlie the source of hard X-ray and microwave emission. It has been shown that the spectral evolution of hard X-rays and microwaves, including peak time delays greater than 1 min, can be consistently explained by the combination of long-lasting injection and trapping of electrons in magnetic loops extending to great heights and containing a plasma of low density. The response to the electron injections at different radio wavelengths (centimetric to metric) varies in the course of the event, and this is attributed to a time-varying access of the energetic electrons to the different sites of emission. The expansion and likely destabilisation of magnetic structures in the middle corona, roughly 0.3 to 0.5 $R_\odot$ above the photosphere, is demonstrated by the observation of a moving type IV radio burst. We discuss in the following two basic assumptions implied in our model calculations, namely those of constant ambient density and of high trapping efficiency. We then put the event of 26 April, 1981 into the context of other hard X-ray bursts, exhibiting impulsive or gradual behaviour, and finally discuss the role of the large-scale magnetic structures involved in the determination of the peculiar properties of gradual bursts.

3.1. Variation of the Ambient Density

In the present study any temporal variation of the density in the X-ray source such as its increase due to chromospheric evaporation has been neglected. Such density variations, which could act on time scales of the order of a few minutes, can modify the delays of high-energy X-rays (and thus probably also of microwave fluxes) with respect to those predicted in the case of a static trap (MacKinnon, 1986). No observations are available to demonstrate that evaporation actually occurs in the present case. However, the observations of other gradual hard X-ray flares have shown that blueshifts or broadenings of soft X-ray emission lines, which may be considered as an indication of chromospheric evaporation (Acton *et al.*, 1982; Doschek *et al.*, 1986), are either absent or very weak in the case of gradual flares: the rise of the soft X-ray line and continuum emissions is steady during the gradual hard X-ray burst, and there is no correlation with the hard X-ray peak, in contrast with the behaviour in impulsive flares, indicating a weaker link between the high-energy particles and the hot flaring plasma (Tanaka, 1987; Dennis, Uberall, and Zarro, 1991).

Another cause of ambient density increase, especially in source 1, lies in the total number of electrons injected in the source. Indeed, at the end of injection 1, 1.44×10^{38} electrons have been injected in the region and partially thermalized. This leads to an increase of the thermal density in the medium which will depend on the overall volume of the trap. We estimate the volume by considering an upper limit of the nonthermal-to-thermal density ratio. The total number of energetic electrons

above 20 keV which are *instantaneously* present is 6×10^{36} at most. If one requests that the density of the energetic electrons be at no instant higher than 10% of the ambient electron density, the volume of the trap must be at least 6×10^{28} cm^3. The (unknown) low-energy cutoff of the injection spectrum of the nonthermal electrons is evidently a key parameter in these estimations. If, as suggested by Cliver *et al.* (1986) who study the evolution of the photon spectrum of the 26 April, 1981 event, there is a significant hot thermal component at photon energies above 35 keV, the density of nonthermal electrons and consequently the inferred volume of the hard X-ray source will be greatly reduced with respect to our value. Although rather large, the derived volume is similar to that inferred from stereoscopic observations of a large hard X-ray burst by Kane *et al.* (1992). Under these conditions the ambient density increase due to the thermalization of the energetic electrons will be at most of the order of 2×10^9 cm^{-3}. Numerical estimations show that the temporal evolutions of the computed X-ray and microwave fluxes are not very sensitive to a slow increase of the ambient density in source 1 (cf. Section 2.5.3).

The combination of evaporation and thermalization can lead to a density twice to four times higher at the end of the injection than at the beginning, provided the source volume is roughly constant. This would lead to a quicker decay of the microwave emission after $\simeq$12:10 UT. If, on the other hand, the volume of the hard X-ray source is ten times bigger, as is the case of the large occulted flare reported by Kane *et al.* (1992), then the increase of the thermal density in source 1 can be completely neglected and betatron deceleration must be considered as discussed in Section 2.5.3.

It was also assumed here, given the lack of constraints, that the source density is the same for the three injections which are directed into two distinct structures. This hypothesis appears artificial given the higher value of the magnetic field in the second region. However, an increase by a factor of the order of 5 of the density in the second region does not significantly change the X-ray flux for the second and third injections for which delays cannot be easily determined. The relative changes are estimated to be on average (over energies and times) of the order of 10%. The effects are more important at low than at high energies. The X-ray flux at the peak time is slightly increased while the decay is faster. On the other hand, numerical estimations show that the computed microwave emission up to 19.6 GHz is not strongly changed if the density in region 2 is twice the density in region 1. However, the computed flux density at 35 GHz is twice lower than the observed one throughout the phase of maximum emission if the density in region 2 is 10^{10} cm^{-3}. We, therefore, conclude that the ambient density in the compact second source is poorly constrained, but most likely significantly below 10^{10} cm^{-3}.

3.2. Efficiency of Trapping in Coronal Magnetic Structures

The electron trapping efficiency is an important parameter in our model, since if a significant number of electrons precipitate from the trap due to wave-particle interactions, the delays of high-energy emissions (and thus probably also of mi-

crowave fluxes) will be greatly reduced. The conditions for electron storage or precipitation from a coronal trap have been studied by Wentzel (1976) in the case of interactions with whistlers. The electron population may or may not be unstable against whistlers depending on the total number of electrons in the loop and on its characteristics (ambient density, volume, field curvature). A slight change of these parameters can modify the storage (Vilmer, 1985). The non-detection of rapidly varying emission might serve as a hint that precipitation is not an important factor in the dynamics of the energetic electrons in this flare. Furthermore, X-ray observations of 'type C' flares by direct imaging of the low-energy component (Tsuneta *et al.*, 1984) or the stereoscopic observations of behind-the-limb events (Kane *et al.*, 1992) demonstrate that energetic electrons can indeed be efficiently trapped in huge coronal loops.

3.3. THE ELECTRON POPULATION

In order to put the event discussed here into a larger perspective, we compare in Table III characteristic quantities of the energetic electron population with those of other impulsive and gradual events that have been modelled in the same way (Vilmer, Kane, and Trottet, 1982; Trottet and Vilmer, 1984; Vilmer, 1985; Hernandez *et al.*, 1986; Hulot *et al.*, 1992). $N_{\rm tot}$ and $W_{\rm tot}$ are, respectively, the total number and energy content of the electrons above 25 keV, τ is the duration of the electron injection (computed as the time between the start of the first and the end of the last injection, irrespective of how much individual injections overlap). When values are preceded by '>', only a section of the whole event has been analyzed, as indicated in the last column. A low-energy cutoff at 25 keV is imposed for the injection spectrum of nonthermal electrons to be consistent with estimates obtained from a set of SMM hard X-ray observations (Wu *et al.*, 1986). The total number of electrons as well as the total nonthermal energy content deduced for the 26 April, 1981 flare are consistent with the values deduced for other gradual events. It is clear that any such comparison is subject to the assumption that the low-energy cutoff is the same in all events. The cutoff energy cannot presently be measured. Keeping this restriction in mind, we are going to discuss quantitative differences between gradual and impulsive events from the limited sample of Table III.

There is a trend that more electrons are accelerated during gradual than during impulsive hard X-ray/radio bursts. The difference is at most one order of magnitude, and a somewhat bigger difference is noticed between the total energy contents. This confirms the tendency inferred by Kai, Kosugi, and Nitta (1985), considering the relation between 17 GHz and hard X-ray fluxes. Arguing that the lower ambient density in gradual sources must be compensated by an accordingly higher density of nonthermal electrons these authors invoke 10^2 to 10^3 times more electrons in gradual than in impulsive events. This appears too high in the light of our model computations. The mean rate of electron injection and of energy deposition are the same for the two groups of events. Given the usually assumed bigger volume of gradual events this implies that the electrons dump less energy per unit surface into

TABLE III

Nonthermal electrons during impulsive and gradual events

Date	$N_{tot}(25)$	$W_{tot}(25)$ (erg)	τ (s)	N_{tot}/τ (s^{-1})	W_{tot}/τ (erg s^{-1})	Remarks
7 June, 1980	$>2 \times 10^{36}$	$>1.4 \times 10^{29}$	8.5	2.3×10^{35}	1.6×10^{28}	Impulsive (1/7 peaks) (Hulot *et al.*, 1992)
29 June, 1980	1.8×10^{37}	1.1×10^{30}	73	2.0×10^{35}	1.5×10^{28}	Impulsive (Hernandez *et al.*, 1986)
14 Aug., 1979	1.1×10^{37}	7.6×10^{29}	15	7.3×10^{35}	5.1×10^{28}	Impulsive
	1.9×10^{37}	1.5×10^{30}	140	1.4×10^{35}	1.1×10^{28}	Gradual (2 peaks) (Vilmer, Kane, and Trottet, 1982)
26 Apr., 1981	1.2×10^{38}	7.4×10^{30}	1000	1.2×10^{35}	7.6×10^{27}	Gradual (this paper)
27 Apr., 1981	$>1.4 \times 10^{38}$	$>1.2 \times 10^{31}$	212	6.7×10^{35}	5.7×10^{28}	Gradual (1/3 peaks) (Hulot *et al.*, 1992)
13 May, 1981	1.0×10^{38}	5.7×10^{30}	360	2.8×10^{35}	1.6×10^{28}	Gradual (Trottet and Vilmer, 1984)

the chromospheric footpoints than during impulsive flares, in accordance with the fact that no signs of chromospheric evaporation are observed during gradual events (Tanaka, 1987). If the volume of gradual events is 10 to 100 times bigger than that of the impulsive bursts, they may tend to have a lower energy density, but the difference is hard to establish, given the inherent uncertainties of our comparison. Such a difference could be related to similar results for the thermal energy density of soft X-ray 'impulsive' and 'long duration' events by Pallavicini, Serio, and Vaiana (1977).

Kai, Kosugi, and Nitta (1985) state that the microwave richness of gradual events is caused by a more abundant population of relativistic electrons (extending to several MeV) during gradual than during impulsive events. While it is true that the microwave emission in a weak magnetic field comes from the high-energy part of the electron spectrum, we emphasize that the same high-energy spectrum would be undetectable at centimetric wavelengths in a strong field because there the gyrosynchrotron emission at the given frequency comes from the low-energy range only. This is borne out by Figure 3 of Kai, Kosugi, and Nitta (1985) which illustrates that in strong magnetic fields the gyrosynchrotron emissivities for electron spectra with cutoffs at 1 and 10 MeV become indistinguishable. The sensitivity of gradual microwave emission to the high-energy part of the electron spectrum is thus a consequence of the injection into extended loops with weak fields and not necessarily the signature of a more pronounced relativistic electron population in gradual events.

3.4. Large-scale changes of the coronal field and the peculiarities of gradual bursts

Gradual hard X-ray/radio bursts usually have signatures over a broad band of radio waves extending from centimetric to metric (flare continua). At first glance the 26 April, 1981 event appears as a counterexample in that the metre wave emission (169 MHz) fades much earlier than the centimetric emission. The decomposition into elementary particle injections, however, shows that this discrepancy can be explained by varying access of the energetic electrons to different coronal structures in the course of the event: during the most energetic first electron injection, emissions extend over a large bandwidth, with a globally similar time profile. During the subsequent injections, no response is detected at metre waves, and the microwave spectrum indicates that regions with more intense magnetic fields become dominant. The varying access to magnetic structures can plausibly result from the evolution of the large-scale plasma-magnetic field configuration, including the ejection of an extended loop or a plasmoid visualized by a moving type IV burst at 169 MHz.

Whether or not this profound modification of the magnetic field structure is the direct cause of the electron acceleration is not clear, however. Cliver *et al.* (1986) locate the acceleration in a neutral sheet underneath the ejected filament material. The accelerating site rises with the filament in the corona. Tanaka (1987)

concludes from the observed positional shift of the hard X-ray source in a gradual event that subsequently higher loops (range 6×10^4 to 9×10^4 km) are activated. Our analysis cannot reveal differences on such relatively small spatial scales. It suggests, however, that in the later phase of the event the injection of electrons is directed into *lower* coronal structures than during the rising and early maximum phase. The analysis of the 26 April, 1981 event seems to imply a multiple-loop structure of which the hard X-ray/microwave sources outline the lower parts while the metric emission comes from the upper part (0.3 to 0.5 $R_\odot$ above the photosphere). During the evolution of the event, the upper part of this complex becomes disconnected, and the metric component of the flare continuum ceases. The multiple-loop picture is favoured by the observation that as one goes from microwaves to lower frequencies the response to the late electron injections becomes *gradually* less pronounced. This is not easy to understand in a single large-scale loop (Kai *et al.*, 1986; Kai, Kosugi, and Nitta, 1983), where all frequencies are expected to show globally the same behaviour. Also the configuration advocated by Cliver *et al.* (1986, Figure 10) where two different traps – one below and one above the neutral sheet – are involved, suggests rather an abrupt distinction between microwaves and metric waves than a gradual transition.

In the case of a high trapping efficiency for electrons up to energies of some MeV, the global evolution of the plasma-magnetic field configuration allows for betatron deceleration, which turns out to be an efficient loss mechanism not considered in gradual hard X-ray/microwave bursts before.

The changing coronal structure is thus a plausible interpretation of several aspects of gradual bursts. The combination of long-lasting injection and trapping of electrons in such structures can account for the similarities in the temporal evolution over a wide spectral band. The evolution of the plasma-magnetic field configuration, on the other hand, implies that there is not always a simple correspondence between different spectral ranges.

Acknowledgements

The authors are grateful to Drs G. Trottet and A. Magun for valuable discussions. G. Bruggmann acknowledges financial support of the European Astrophysical Doctoral Network for his visits to the 'Observatoire de Paris'. The work at the Institute of Applied Physics at Bern was supported by the Swiss National Science Foundation under grant No. 20–25533–88. We acknowledge with thanks the help of Jon Loran in processing the ISEE-3 data, and of J. M. Robillot who made the Bordeaux decimetric data available. The research at the University of California at Berkeley was supported by NASA under grant NAG5–376 and NAGW-2452. We also acknowledge the comments of unknown referees that led to many improvements of this work.

References

Acton, L. W., Canfield, R. C., Gunkler, T. A., Hudson, H. S., Kiplinger, A. L., and Leibacher, J. W.: 1982, *Astrophys. J.* **263**, 409.

Bai, T.: 1982, in R. E. Lingenfelter, H. S. Hudson, and D. M. Worall (eds.), *Gamma-Ray Transients and Related Astrophysical Phenomena*, A.I.P., New York, p. 315.

Bai, T. and Dennis, B. R.: 1985, *Astrophys. J.* **292**, 699.

Bai, T. and Ramaty, R.: 1979, *Astrophys. J.* **219**, 705.

Bai, T. and Sturrock, P. A.: 1989, *Ann. Rev. Astron. Astrophys.* **27**, 421.

Bai, T., Hudson, H. S., Pelling, A. M., Lin, R. P., Schwartz, R. A., and von Rosenvinge, T. T.: 1983, *Astrophys. J.* **267**, 433.

Cliver, E. W., Kahler, S. W., and McIntosh, P. S.: 1983, *Astrophys. J.* **264**, 699.

Cliver, E. W., Dennis, B. R., Kiplinger, A. L., Kane, S. R., Neidig, D. F., Sheeley, N. R., Jr., and Koomen, M. J.: 1986, *Astrophys. J.* **305**, 920.

De Jager, C. and de Jonge, G.: 1978, *Solar Phys.* **58**, 127.

Dennis, B. R.: 1985, *Solar Phys.* **100**, 465.

Dennis, B. R.: 1988, *Solar Phys.* **118**, 49.

Dennis, B. R., Uberall, B. M., and Zarro, D.: 1991, in Z. Švestka, B. V. Jackson, and M. E. Machado (eds.), *Eruptive Solar Flares, Lecture Notes in Physics* **399**, p. 199.

Doschek, G. A., Antiochos, S. K., Antonucci, E. *et al.*: 1986, in M. Kundu and B. Woodgate (eds.), *Energetic Phenomena on the Sun*, NASA-CP 2439.

Dulk, G. A.: 1973, *Solar Phys.* **32**, 491.

Hernandez, A. M., Machado, M. E., Vilmer, N., and Trottet, G.: 1986, *Astron. Astrophys.* **167**, 77.

Hulot, E., Vilmer, N., Chupp, E. L., Dennis, B. R., and Kane, S. R.: 1992, *Astron. Astrophys.* **256**, 273.

Kahler, S. W.: 1984, *Solar Phys.* **90**, 133.

Kai, K., Kosugi, T., and Nitta, N.: 1985, *Publ. Astron. Soc. Japan* **37**, 105.

Kai, K., Nakajima, H., Kosugi, T., and Kane, S. R.: 1983, *Solar Phys.* **86**, 231.

Kai, K., Nakajima, H., Kosugi, T., Stewart, R. T., Nelson, G. J., and Kane, S. R.: 1986, *Solar Phys.* **105**, 393.

Kane, S. R., McTiernan, J., Loran, J., Fenimore, E. E., Klebesadel, R. W., and Loras, J. G.: 1992, *Astrophys. J.* **390**, 687.

Kawabata, K., Ogawa, H., Takakura, T., Tsuneta, S., Ohki, K., Yoshimori, M., Okudaira, K., Hirashima, Y., and Kondo, I.: 1982, *Hinotori Symp. on Solar Flares*, ISAS, Japan, p. 168.

Klein, K.-L.: 1987, *Astron. Astrophys.* **183**, 341.

Klein, K.-L., Trottet, G., and Magun, A.: 1986, *Solar Phys.* **104**, 243.

Klein, K.-L., Anderson, K., Pick, M., Trottet, G., Vilmer, N., and Kane, S. R.: 1983, *Solar Phys.* **84**, 295.

Klein, K.-L., Trottet, G., Benz, A., and Kane, S. R.: 1988, *ESA-SP* **285**(1), 157.

Kosugi, T., Dennis, B. R., and Kai, K.: 1988, *Astrophys. J.* **324**, 1118.

Kosugi, T., Kai, K., and Suzuki, T.: 1983, *Solar Phys.* **87**, 373.

MacKinnon, A. L.: 1986, *Astron. Astrophys.* **163**, 239.

MacKinnon, A. L., Brown, J. C., Trottet, G., and Vilmer, N.: 1983, *Astron. Astrophys.* **119**, 297.

Nakajima, H.: 1983, *Solar Phys.* **86**, 427.

Ohki, K., Takakura, T., Tsuneta, S., and Nitta, N.: 1983, *Solar Phys.* **86**, 301.

Pallavicini, R., Serio, S., and Vaiana, G. S.: 1977, *Astrophys. J.* **216**, 108.

Pick, M.: 1986, *Solar Phys.* **104**, 19.

Ramaty, R.: 1969, *Astrophys. J.* **158**, 753.

Takakura, T., Tsuneta, S., Ohki, K., Nitta, N., Nakishima, K., Murakami, T., Ogawara, Y., Oda, M., and Miyamoto, S.: 1983, *Astrophys. J.* **270**, L83.

Tanaka, K.: 1987, *Publ. Astron. Soc. Japan* **39**, 1.

Trottet, G.: 1986, *Solar Phys.* **104**, 145.

Trottet, G. and Vilmer, N.: 1983, *Proc. 18th Int. Cosmic Ray Conf., Bangalore*, SP 3-15.

Trottet, G. and Vilmer, N.: 1984, *Adv. Space Res.* **4**(7), 153.

Tsuneta, S., Takakura, T., Nitta, N., Ohki, K., Makishima, K., Murakami, T., Oda, M., and Ogawara, Y.: 1984, *Astrophys. J.* **280**, 887.

Vilmer, N.: 1985, 'Etude de l'accélération et du piégeage des électrons lors des éruptions solaires à partir des émissions de rayonnement X et radioélectriques', thèse, Univ. de Paris VII, France.
Vilmer, N: 1987, *Solar Phys.* **111**, 207.
Vilmer, N., Kane, S. R., and Trottet, G.: 1982, *Astron. Astrophys.* **108**, 306.
Vilmer, N., MacKinnon, A. L., Klein, K.-L., and Trottet, G.: 1987, *Proc. 20th Int. Cosmic Ray Conf., Moscow*, SH-2.1-2.
Wentzel, D. G.: 1976, *Astrophys. J.* **208**, 595.
Wu, S. T., de Jager, C., Dennis, B. R., Hudson, H. S. *et al.*: 1986, in M. Kundu and B. Woodgate (eds.), *Energetic Phenomena on the Sun*, NASA-CP 2439.
Yoshimori, M., Watanabe, H., and Nitta, N.: 1985, *J. Phys. Soc. Japan* **54**, 4462.